Aging and Disease
www.aginganddisease.org
Early access date: October 26, 2026
http://dx.doi.org/10.14336/AD.2026.1010

Review

Tissue- and Organ-Related Molecular Aging Clocks: Measurement, Interpretation, and Translational Validation

Ting Wang[1#], Shiqing Xie[1#], Lihua Yu[1,2*], Ting Xu[1,2*]

[1]Clinical Laboratory, the Affiliated Yongchuan Hospital of Chongqing Medical University, Chongqing, China.
[2]General Practice School of Chongqing Medical University, Chongqing, China.

[Received August 14, 2026; Revised October 7, 2026; Accepted October 7, 2026]

ABSTRACT: Biological age measures are increasingly derived from target tissues, proximal fluids, and circulating signals, but whether they represent aging of a specific organ remains uncertain. Differences in sample source, biological resolution, and validation make predicted ages and age gaps from these pathways non-interchangeable. This critical narrative review compares representative molecular clocks of the central nervous system and peripheral organs and introduces the source, resolution, and validation framework, abbreviated as S–R–V, to assess the organ attribution and translational claims supported by each model. Across organs, molecular age measures were linked to different aspects of organ state and biological context. Chronological age prediction was more consistently demonstrated than alignment with organ pathology or function. Age gaps may reflect varying contributions from organ-related signals, cellular composition, systemic influences, disease-related remodeling, and technical or modeling effects. Correlations among organ age gaps represented dependence among model outputs and did not establish communication, temporal ordering, or causality between organs. Evidence was concentrated in model development, external replication, and cross-sectional disease association, while prospective prediction, longitudinal responsiveness, and clinical utility were less developed. Future studies should pair target tissue, proximal fluid, and circulating measures with organ pathology or function in the same participants and use repeated measurements to determine whether accessible measures track within-person change. By matching measurement context to validation evidence, S–R–V can help define when organ age measures support risk stratification, longitudinal monitoring, or intervention evaluation.

Keywords: tissue- and organ-related molecular aging clocks, biological age, epigenetic clocks, age gap, organ aging heterogeneity, translational validation

1. Introduction

Aging is an important risk factor for numerous chronic diseases, including cardiovascular disease, neurodegenerative disorders, and malignancies [1]. Chronological age reflects the passage of time, whereas biological aging involves progressive molecular and cellular changes across multiple interconnected processes [2]. Early molecular aging models, exemplified by DNA methylation clocks, were trained primarily to predict chronological age [3, 4]. Subsequent studies gradually incorporated clinical phenotypes, mortality risk, and healthspan into model development or validation, extending the application of aging clocks from age prediction to health risk assessment [5–8]. DunedinPACE was developed to quantify the pace of aging [9], whereas principal component–based clocks were designed to improve measurement reliability in longitudinal studies and clinical trials [10]. Despite these advances, accurate

***Correspondence should be addressed to:** Ting Xu (Email: xuting@hospital.cqmu.edu.cn) and Lihua Yu (Email: YLH@hospital.cqmu.edu.cn), Clinical Laboratory, the Affiliated Yongchuan Hospital of Chongqing Medical University, Chongqing 402160, China. #* These authors contributed equally to this work.

Copyright: © 2026 Wang T. et al. This is an open-access article distributed under the terms of the Creative Commons Attribution License, which permits unrestricted use, distribution, and reproduction in any medium, provided the original author and source are credited.

age prediction does not necessarily mean that a model measures a biologically meaningful aging process; its interpretation still depends on the training target, signal source, and evidence from external validation.

Human aging does not progress synchronously across all organs. Tissues differ in cellular composition and regenerative capacity and are exposed to distinct metabolic burdens and environmental stressors, giving rise to different aging trajectories. These trajectories are also shaped by shared systemic aging processes [11]. Pan-tissue or peripheral blood clocks can capture systemic aging to some extent but cannot establish whether local age-related changes have occurred in a specific organ. Expanding human tissue resources and high-resolution cellular atlases have made it possible to examine age-related changes at the level of individual organs and their constituent cell populations [12–15]. These resources and technological advances have driven the development of a growing number of age models tailored to specific tissues and organs. Such models typically generate a predicted age, from which a deviation measure relative to chronological age is derived as an index of individual-level variation in biological aging. In this review, age gap is used as an umbrella term for such measures; their statistical definitions vary across studies and are detailed in Section 4.1. However, identifying an organ-associated age deviation does not establish that a model measures aging of the organ itself. Moving from "organ-related" to "organ-specific" requires independent validation, biological anchoring, and evidence distinguishing target organ signals from shared systemic signals or signals from other organs.

Recent reviews and perspectives have examined the clinical promise, organ-specific measurement, and emerging technologies of biological aging clocks from complementary perspectives. One recent review critically appraised biological aging clocks and their potential roles in understanding pathobiology, reducing disease burden, and extending healthspan [16]. An organ-specific perspective outlined methods for measuring organ-specific biological age, synthesized evidence on heterogeneous and interconnected organ aging, and proposed research priorities including longitudinal tracking, biomarkers with high organ specificity, and reference ranges for organ age gaps [17]. Another review evaluated existing multi-omics and imaging approaches to organ biological age assessment and highlighted quantum sensing as an emerging strategy for detecting early and subtle changes in organ microenvironments [18]. Complementary biomarker frameworks address related but distinct questions. The FDA–NIH Biomarkers, EndpointS, and other Tools (BEST) resource harmonizes biomarker categories and terminology according to intended use and context of use [19]. The Biomarkers of Aging Consortium subsequently advanced a framework for aging-biomarker terminology, classification, potential clinical use cases, and analytical and clinical validation [20], while later work focused more specifically on predictive validity, cross-cohort comparability, and population-level generalizability [21]. However, prior work has not integrated anatomical signal source, biological resolution, and the maturity of organ attribution evidence within a unified cross-model framework or systematically linked these dimensions to the claims supported by each model.

To address this gap, we propose a claim-centered source–resolution–validation (S–R–V) assessment framework. Here, claim-centered means that each model is evaluated according to the level of organ attribution and intended-use claims justified by the available evidence, rather than by age-prediction performance alone. S (source) identifies the origin of the biospecimen and its anatomical relationship to the target organ. R (resolution) classifies the biological level at which the signals used to construct or calculate the age estimate are resolved. R1–R4 distinguish bulk or mixed samples, computationally resolved cell-type information with donor- or tissue-level age estimation, physically isolated cell populations or tissue compartments, and individual-cell or individual-nucleus age estimates, respectively. These categories generally reflect increasing cellular specificity, whereas R5 captures preserved spatial context and may operate at multicellular, cellular, or subcellular scales; R5 should therefore not be interpreted as inherently higher than R4. V (validation) denotes the maturity of evidence supporting organ attribution and translational claims, with each validation domain (V1–V6) assessed independently. Standardized terminology for organ attribution is provided in Supplementary Table S5. We apply this framework to compare representative models and evaluate the degree of organ attribution supported by different measurement pathways. We also examine the biological components of age gaps, synthesize evidence on cross-organ aging relationships, and discuss the validation evidence needed to support disease-association and clinical-application claims for organ age measures.

This critical narrative review draws on literature searches in PubMed and the Web of Science Core Collection through 3 September 2026. Search terms covered molecular aging clocks and age-prediction models across different anatomical sources and molecular modalities. Peer-reviewed original human studies were eligible if they developed, validated, or directly applied a molecular model yielding a predicted age, age-acceleration measure, or explicit tissue- or organ-level biological-age estimate. After deduplication, 840 unique PubMed/Web of Science records were screened, yielding 143 eligible studies identified through the database

searches. Additional relevant studies were identified through citation chaining, targeted model-name searches, and supplementary Google Scholar searches. These supplementary procedures identified 35 additional eligible studies, resulting in a final evidence base of 178 reports. Animal, organoid, and in vitro studies were retained only as clearly separated mechanistic, technical, or intervention context and were not included in this denominator. Detailed search strategies, eligibility criteria, and study-flow information are provided in the Supplementary Methods and Supplementary Figure S1. The complete inventory of eligible human studies is provided in Supplementary Table 6.

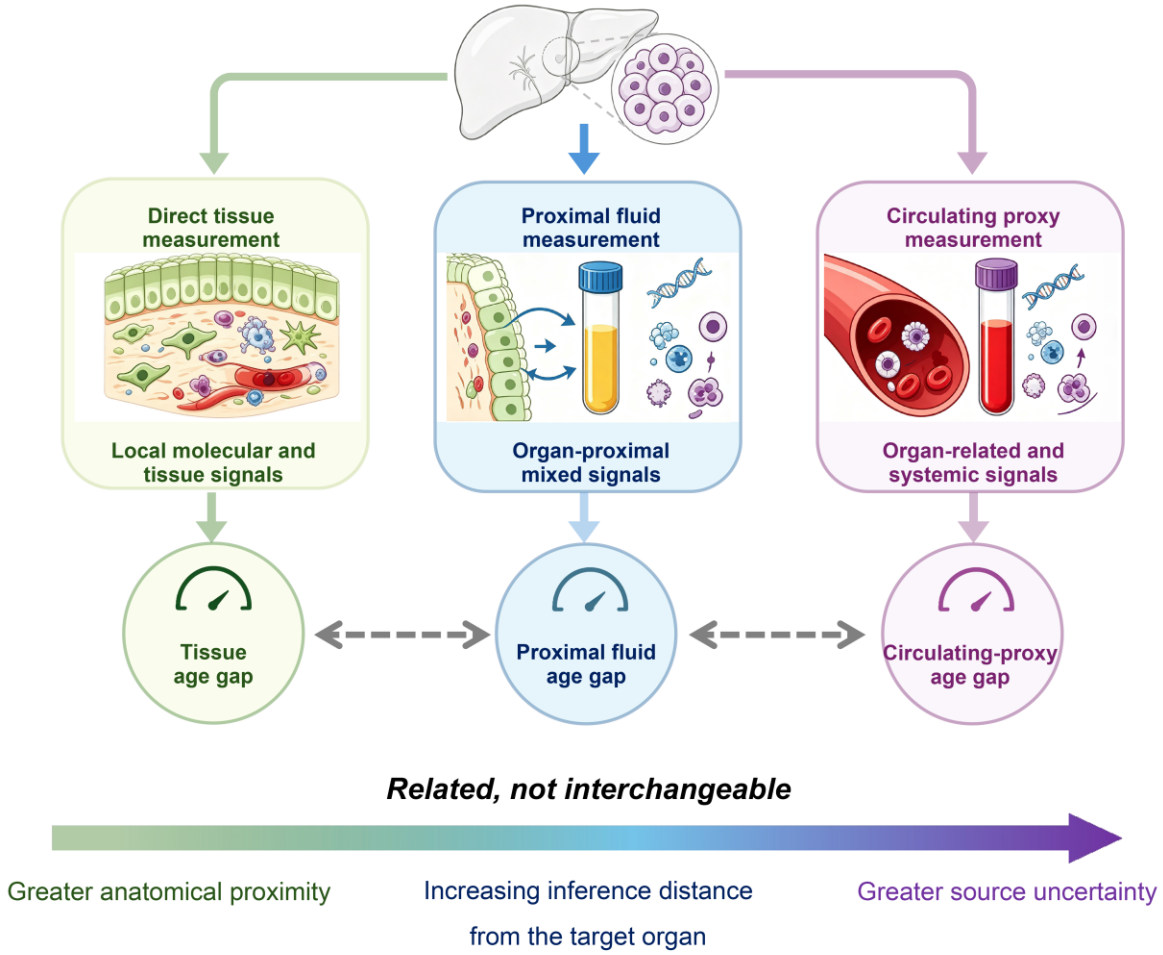


Figure 1. Measurement pathways generate related but non-interchangeable age gap estimates. Age gap is used here as an umbrella term for the deviation of model predicted age from chronological age. Direct tissue, proximal fluid, and circulating proxy measurements capture local tissue signals, mixed signals from the target organ and nearby compartments, and organ related signals mixed with systemic circulating signals, respectively. Dashed bidirectional arrows indicate possible statistical dependence between estimates, but the estimates are not interchangeable and do not establish organ-to-organ communication, temporal ordering, or causality. Organ attribution becomes less direct, and source uncertainty increases from direct tissue measurement to circulating proxy measurement.

The S–R–V assignments were intended as structured and transparent interpretations of the reported evidence rather than as formal evidence grades or risk-of-bias assessments. S and R codes were assigned based on the biospecimen source and biological resolution, respectively, and V categories were assigned according to the validation domains evaluated in the original studies. Each V category was assigned when its corresponding evaluation criterion was met, irrespective of whether other categories were satisfied. If the original report did not provide enough information to determine S or R, the corresponding dimension was left unclassified.

Because molecular aging models differ in what they are trained to estimate, the S–R–V framework does not impose identical validation requirements across model types. For models trained to predict chronological age, V2 specifically denotes independent age-prediction performance; models trained on other aging-related

targets, such as phenotypic-age, mortality-risk, or longitudinal pace-of-aging measures, are not assigned this category unless that criterion is satisfied. Phenotypic, prospective, intervention-response, and decision-impact evidence are recorded separately as V3–V6, irrespective of the model's original training target.

2. Measurement Pathways and Interpretive Boundaries of Tissue and Organ Aging Clocks

The biological meaning of tissue and organ aging clocks depends on where the measured signals originate and the biological level that a model can resolve. These two considerations correspond to the S and R dimensions, respectively, in the S–R–V framework. Measurement pathways differ in anatomical proximity, the degree of signal mixing, and susceptibility to systemic confounding, each presenting distinct strengths and limitations. Figure 1 summarizes the measurement pathways and their overall relationships, and Table 1 provides the corresponding classification criteria.

2.1 Direct Measurement of Target Tissues Across Bulk-Tissue, Cellular, and Spatial Scales

Early tissue-derived epigenetic clocks were typically developed using bulk tissue obtained at autopsy, surgical resection, or biopsy. Regularized regression and related methods were used to select molecular features associated with chronological age and construct tissue-derived age-prediction models [22]. Such models capture both age-related molecular changes within specific cell types and shifts in the relative abundance of cell types associated with age, disease, or tissue remodeling [23]. Changes in cellular composition, which may arise from processes such as immune-cell infiltration, loss of parenchymal cells, or expansion of fibrosis-associated cell populations, can alter estimates of cell-intrinsic aging. At the same time, these changes may themselves constitute part of tissue aging and pathological remodeling. Whether cellular composition should be adjusted for depends on the research objective. If the overall state of the tissue is of interest, compositional changes may be retained as part of the age-related signal. If the objective is to resolve intrinsic aging within a particular cell type, changes in cell proportions must be distinguished from intracellular molecular changes.

Computational deconvolution offers a compromise for resolving cell-type signals in complex tissues without physical separation. Reference profile–based methods, exemplified by the Houseman algorithm, can estimate cellular composition in bulk samples, and these estimates can be incorporated into models as covariates to reduce the influence of differences in cell proportions on age prediction [24]. Subsequent approaches have moved beyond simply adjusting for cellular composition toward identifying cell type–specific age-related changes. For example, CellDMC identifies cell type–specific differentially methylated positions by modeling interactions between cell proportions and age, whereas multi-omics deconvolution methods broaden the range of data modalities amenable to analysis [25–28]. However, the validity of these attributions depends on the cell types represented in the reference profiles, the correspondence between the reference data and target samples, and the stability of cellular phenotypes under aging or disease conditions. Deconvolution can strengthen interpretation at the cell-type level, but its results remain model-based inferences and cannot be equated with physical cell sorting or direct single-cell measurements.

Table 1. Operational S–R–V classification framework for tissue- and organ-related biological age models

Dimension	Category	Operational criterion
Anatomical source (S)	S1: Direct target tissue	The model is calculated from tissue or cells obtained directly from the target organ.
	S2: Organ-proximal sample	The model is calculated from a biofluid or local output in direct anatomical or physiological relation to the target organ, with the output explicitly defined as reflecting that organ's age.
	S3: Peripheral organ-attributed proxy	The model is calculated from a peripheral circulating sample, with organ attribution explicitly established through organ-enriched features or organ-specific model construction.
Biological resolution (R)	R1: Bulk or mixed sample	The age estimate is calculated from bulk molecular measurements without cell-type resolution.
	R2: Computationally resolved	Cell-type-specific information is resolved computationally, with age estimated at the donor or tissue level.

	R3: Physically isolated	A defined cell population or tissue compartment is physically isolated before molecular profiling.
	R4: Single-cell or single-nucleus	The age estimate is constructed or calculated at the level of individual cells or nuclei.
	R5: Spatially resolved	Spatial coordinates or local tissue context are retained when constructing or calculating the age estimate.
Validation domain (V)	V0: Development only	The model is fitted or calibrated, but none of the evaluations defined under V1–V6 is reported.
	V1: Internal validation	Performance is evaluated by cross-validation, bootstrap, resampling, or a held-out subset drawn from the development data source.
	V2: Independent external evaluation	The fixed model is evaluated for age-prediction performance in an independent dataset not used for feature selection, model fitting, or calibration.
	V3: Target organ phenotypic evaluation	The fixed model is evaluated against an explicitly reported target organ phenotype, including histopathologically confirmed tissue lesion status or grade, structural or imaging measures, physiological function, or molecular pathology. A clinical diagnosis or patient-level case–control label without direct organ phenotyping is insufficient.
	V4: Prospective outcome evaluation	The fixed model is evaluated prospectively against subsequent target organ disease onset, progression, or functional decline.
	V5: Intervention-response evaluation	The fixed model output is evaluated following a deliberately administered intervention, including clinical, behavioral, pharmacological, or experimental interventions.
	V6: Decision-impact evaluation	The model is used to inform a clinical or operational decision, and its effect on decisions, outcomes, or resource use is evaluated.

Notes: Each model was assigned to one S category and one R category according to the biospecimen and resolution at which its age estimate was calculated; use of higher-resolution data only for validation did not change the R category. V categories were non-cumulative and were listed individually; V0 was used only when none of V1–V6 was met. Assignment of V1–V6 recorded whether the corresponding evaluation was performed, irrespective of whether the result was supportive, null, or mixed. Evidence was combined across applications of the same fixed model.

Physical cell sorting and laser-capture microdissection can clarify signal origin at the level of specific cell types or tissue compartments, although the resulting measurements generally remain averages across sorted cell populations or localized compartments. Single-cell and single-nucleus omics enable molecular measurements at the level of individual cells or nuclei. Compared with bulk data, single-cell and single-nucleus data preserve information on cell type and cell state during model development, facilitating the detection of heterogeneity obscured by tissue-level averaging [29, 30]. However, the granularity of model output depends on how the data are aggregated and how the model is trained. Outputs may take the form of individual-cell or individual-nucleus estimates, cell type–specific pseudobulk estimates, or donor-level estimates. The use of single-cell or single-nucleus data therefore does not automatically confer single-cell-level output or interpretation. Beyond output granularity, single-cell clock development and evaluation must also account for the donor structure of the data [31]. Single-cell transcriptomic data are sparse and can be sensitive to batch effects and cell-annotation quality [32–34]. Cells derived from the same donor share donor-specific biological and technical characteristics and therefore do not constitute independent experimental units. Treating these cells as independent replicates creates pseudoreplication, whereas random cell-level partitioning can place cells from the same donor in both the training and test sets, thereby introducing data leakage [35]. Training and test sets should therefore be partitioned at the donor level [31, 35]; increasing the number of cells does not increase the independent sample size.

Spatial omics methods preserve anatomical location, neighborhood composition, and local tissue architecture, allowing investigators to assess whether age-related changes are concentrated within particular compartments or pathological regions [36–41]. The principal value of these models lies not simply in improving age-prediction accuracy, but in linking cellular states to the local microenvironment. Nevertheless, their results remain sensitive to spatial resolution, tissue coverage, and platform differences, and the stability and transferability of local age signals require further validation.

Target tissue models may also be affected by sample selection and preanalytical conditions. Tissue dissociation

and storage can alter measured gene expression and apparent cell-type composition [42], whereas death and post-mortem cold ischemia can induce tissue-specific transcriptomic changes [43]. Autopsy, surgical resection, and biopsy specimens also arise from different clinical contexts, so age may be entangled with disease burden and other characteristics of the sampled population. Models may therefore capture signals that covary with age within a particular sampling frame but do not fully represent normal aging. Cross-study comparisons of tissue-derived models and their age gaps should avoid directly attributing differences between models to organ aging trajectories. As biological resolution increases, the biological question becomes more specific and the technical demands grow. Study design should therefore balance finer localization with adequate independent-donor replication and representative sampling of tissue regions and cell types, while robustness across platforms and datasets should be evaluated explicitly.

2.2 Organ Age Inference from Proximal Biofluids and Peripheral Circulating Proxies

Solid-tissue clocks have a relatively well-defined anatomical origin, but the need for tissue sampling limits their application in large-scale population studies and longitudinal follow-up. Although proximal biofluids such as cerebrospinal fluid are closer to the target organ environment than peripheral blood, they still integrate signals from multiple anatomical compartments and are influenced by secretion, barrier permeability, and clearance. They therefore cannot be considered direct substitutes for solid tissue [44, 45].

High-throughput plasma proteomic platforms can measure thousands of proteins simultaneously, making multi-organ age inference feasible at the population scale [46–48]. Existing organ protein clocks typically use tissue expression atlases such as the Genotype-Tissue Expression (GTEx) project to identify genes that are relatively enriched in the target organ and then map them to features available on plasma proteomic platforms, thereby defining candidate sets of organ-associated features [48]. These proteins may enter the circulation through active secretion, cell turnover, or tissue damage, but their circulating abundance is also shaped by transport, degradation, and clearance [48–50]. The selected protein features are subsequently used to train models of chronological age, from which organ age gaps are derived [48]. High chronological-age prediction accuracy demonstrates that the selected circulating proteins contain age-related information, but neither predictive accuracy nor organ enrichment establishes that these signals are exclusive to, or originate predominantly in, the target organ [48]. Plasma-derived organ age gaps should therefore be interpreted as age deviations inferred from organ-associated circulating molecular patterns rather than as direct measures of the intrinsic molecular age of solid organs.

2.3 Formation and Temporal Heterogeneity of Age-Predictive Signals

The interpretive limits of biofluid measurements also extend to temporal behavior. In a plasma proteomic study of individuals aged 18–95 years, three prominent peaks of age-related change were identified at approximately 34, 60, and 78 years. Trajectory clustering further showed that age-related protein changes followed not only linear patterns but also stepwise, logarithmic, and exponential trajectories [47]. Paired proteomic analysis of cerebrospinal fluid (CSF) and plasma further found that, among healthy controls, the CSF-to-plasma ratios of many proteins changed with age in a protein-specific manner, indicating that molecular relationships between the CSF and plasma compartments are also age dependent [45]. Thus, age-related trajectories observed in biofluids may reflect both molecular changes in source compartments and age-dependent shifts in intercompartmental relationships.

DNA methylation studies provide complementary empirical and modeling evidence on how age-predictive relationships may arise. Comparisons of tissue-level and single-cell DNA methylation dynamics in mice indicate that epigenetic aging comprises both coordinated changes and a substantial stochastic component [51]. Simulation studies further show that when molecular states progressively diverge from an initial state over time, stochastic variation alone can be sufficient to construct an aging clock [52]. Evidence also suggests that stochastic methylation changes may account for a substantial proportion of chronological-age prediction accuracy, whereas their relative contribution to biological-age prediction appears lower; the relative contributions of stochastic and non-stochastic components vary across models [53].

In a cross-age atlas of 17 mouse organs and plasma, age-related molecular changes followed both linear and nonlinear trajectories, while the magnitude and timing of changes in the same biological processes differed across organs [54]. Paired transcriptomic and proteomic analyses of the same tissue homogenates from mice further showed that significant age-related changes in mRNA and protein abundance were only partially concordant across molecular layers, with post-transcriptional dysregulation becoming more evident after 24 months of age [55]. Collectively, these findings indicate that age-related molecular signals are heterogeneous in their formation

mechanisms, molecular layers, and trajectories across the life course.

3. Evidence Landscape and Validation Gaps for Molecular Aging Clocks Across Organs

Section 3 applies the S–R–V framework to representative organ studies, with the corresponding classifications summarized in Table 2. Detailed phenotypic, prospective, and intervention evidence underlying the V3–V5 assignments is provided in Supplementary Table S1, while Supplementary Table S2 situates these representative models within the broader landscape of same-lineage applications and selected alternative models. The comparison focuses on the biological attribution and translational claims supported by each model's evidence base.

Table 2. Representative tissue- and organ-related molecular aging models classified using the S–R–V framework.

Organ/level	Representative model and modality	Species/sample and external evaluation	S–R–V profile	Validation evidence	Key confounder/ evidentiary boundary
Human evidence					
Brain—cortex	DNAmClockCortical [56, 57] (DNA methylation)	Human; development n=1,397; independent cortical evaluation n=1,221	S1–R1; V1, V2, V3	Selected AD neuropathology and cognitive outcomes: **supportive**; cerebral infarcts: **null**; cerebral atherosclerosis: significant inverse association	Post-mortem observational evidence
Brain—cerebellum	CerebellumClock specific [59, 105] (DNA methylation)	Human; development n=752; independent age-prediction evaluation n=24	S1–R1; V1, V2	No cerebellum-localized V3 evaluation	Small independent cohort
Brain—neurons/glia	Neuron- and glia-specific DNAm clocks [60] (DNA methylation)	Human; development n=416; model-selection n=67; independent sorted-neuron validation n=143 across five datasets	S1–R2; V1, V2	Independent age-prediction performance	Cell-type information computationally resolved
Brain—single nuclei	Cell-type-specific transcriptomic aging clocks [62] (snRNA-seq)	Human; 31 donors, 73,941 nuclei; independent datasets evaluated	S1–R4; V1, V2,V3	Independent age-prediction performance; ADNC-defined group differences: **supportive** in oligodendrocytes and microglia, **null** in other cell types	Development data were PFC-based (31 donors)
Brain—CSF	CSF proteomic clock [44] (proteomics)	Human; development n=437; independent ADNI n=735	S2–R1; V1, V2, V3	Amyloid-β pathology: **null**	CNS-proximal biofluid rather than direct brain tissue
Multi-organ—plasma	OrganAge organ-specific clocks [48, 106–108] (proteomics)	Human; development n=1,398; multiple independent cohorts	S3–R1; V1, V2, V3,V4,V5	Phenotypic associations: **mixed**; selected prospective organ–outcome associations: **supportive**; intervention responses: **mixed** across organs	Circulating proxy; V domains apply to evaluated submodels, not every organ clock. Cognition-optimized models remain distinct
Liver	HepClock [60, 63] (DNA methylation)	Human; both developed in n=210 liver samples;	**HepClock**:S1–R2; V1, V2, V3	**HepClock**: MASLD stage and component histopathology **null**.	Small MASLD biopsy cohort; LiverClock had

	LiverClock [60, 63] (DNA methylation)	independent age-prediction evaluation in n=55 primary hepatocyte cultures; MASLD biopsy application n=22	**LiverClock**:S1–R1; V1, V2, V3	**LiverClock**: overall MASLD stage **supportive**; individual histological components **null**	higher age-prediction error than HepClock in primary hepatocytes
Kidney	Kidney EpiAge [65] (DNA methylation)	Human; development n=183	S1–R1; V1, V3	Nephrosclerosis (n=71): greater severity associated with lower EpiAge	No independent age-prediction evaluation
Heart—cardiac/atrial tissue	M&P cardiac clock [67] (targeted CpG pyrosequencing)	Human; cardiac-tissue analysis n=313; overall surgical cohort n=383	S1–R1; V1, V3	Selected ventricular structure/function measures **supportive**; EF and some wall-thickness measures: **null**	Disease-enriched surgical cohort; no independent age-prediction evaluation
Skeletal muscle	**MEAT** [69, 72, 109] (DNA methylation)	Human; **MEAT:** development n=682; independent cohorts n=139 and 47;	**MEAT:** S1–R1; V1, V2, V3, V5	**MEAT:** physical function/fitness mostly **weak or null** after adjustment; HIIT-induced change in age acceleration: **null**.	**MEAT:** Evidence from selected human cohorts and exercise settings
	MEAT2.0 [70, 109–112] (DNA methylation)	Human; **MEAT2.0:** development n=1,053; independent age-prediction evaluations in additional cohorts	**MEAT2.0:** S1–R1; V1, V2,V3, V5	**MEAT2.0:** Quadriceps fat infiltration: **supportive**; muscle area and strength: **null**. Human NR-associated age-acceleration reduction: **supportive;** exercise-training response: **null**	**MEAT2.0:** Disease-context-dependent findings; no concurrent untreated control in the NR trial; small exercise subsets
Musculoskeletal tissues	MskAge [73] (DNA methylation)	Human; assembled model resource n=1,048, including a held-out test set n=307; separate OA cartilage application n=298	S1–R1; V1, V3, V5	OA cartilage: **supportive** in hip, not significant after FDR correction in knee; in vitro reprogramming: **supportive** predicted-age reduction; muscle exercise intervention: **null**	Reprogramming evidence is in vitro; OA and intervention findings varied by tissue and setting
Lung—parenchyma	Lung parenchyma aging clock [77] (scRNA-seq transcriptomics)	Human; n=181 modeled from 184 donors; independent cohorts n=8 and 10	S1–R2; V1, V2	Comparable or superior age-prediction performance in two independent cohorts	Small external cohorts; donor-level output from computationally resolved cell-type modules
Skin—bulk tissue	Skin-specific PathwayAge [84] (DNA methylation)	Human; development n=322; independent external skin cohorts evaluated	S1–R1; V1, V2, V3	Lesional psoriasis and AK/cSCC AgeAcc: **supportive**; primary versus metastatic melanoma: **null** for overall AgeAcc, **mixed** at pathway level	Cross-sectional lesion-defined states rather than prospective progression
Colon	Colon-specific epigenetic clocks [82] (DNA methylation)	Human; development n=210; held-out internal evaluation	S1–R1; V1, V3	Polyp age acceleration: **supportive**; histological grade/subtype associations: **null**	No independent age-prediction evaluation; pathology evidence derived from lesion tissue
Preclinical methodological exemplar					

Brain—spatial, preclinical	Spatial transcriptomic clocks [38] (MERFISH transcriptomics)	Mouse; two independent aging cohorts spanning 20 ages; atlas ≈4.2 million cells	S1–R5; V1, V2, V5	Exercise: **supportive** predicted-age reductions in selected cell types; partial OSKM reprogramming: **mixed** cell-type responses in mice	Preclinical mouse evidence only

Notes: S, R, and V categories are defined in Table 1. V categories are non-cumulative and indicate whether the corresponding validation domain was evaluated, irrespective of whether findings were supportive, null, or mixed. The preclinical spatial-clock row is presented separately as a methodological exemplar. Original model names are retained as reported and do not by themselves indicate that organ-specific attribution has been established. Detailed phenotypic, prospective, and intervention evidence underlying V3–V5 assignments is provided in Supplementary Table S1.
Abbreviations: AD, Alzheimer's disease; ADNC, Alzheimer's disease neuropathologic change; AgeAcc, age acceleration; AK, actinic keratosis; CNS, central nervous system; CSF, cerebrospinal fluid; cSCC, cutaneous squamous cell carcinoma; EF, ejection fraction; FDR, false discovery rate; HIIT, high-intensity interval training; MASLD, metabolic dysfunction–associated steatotic liver disease; MERFISH, multiplexed error-robust fluorescence in situ hybridization; NR, nicotinamide riboside; OA, osteoarthritis; OSKM, OCT4, SOX2, KLF4, and c-MYC reprogramming factors; PFC, prefrontal cortex; scRNA-seq, single-cell RNA sequencing; snRNA-seq, single-nucleus RNA sequencing.

3.1 Multiscale Central Nervous System Clocks

DNA methylation clocks developed specifically for the human cerebral cortex provide more accurate age estimates in cortical samples than pan-tissue or blood-derived clocks and, in some studies, show stronger associations with Alzheimer's disease (AD) pathology, cognitive decline, and dementia [56, 57]. However, greater accuracy in predicting chronological age does not necessarily translate into stronger disease associations. PCBrainAge uses a principal component–based approach to reduce technical noise and improve test–retest reliability. Although it does not provide the most accurate prediction of chronological age, its age-acceleration measure shows stronger associations with clinical AD, AD pathology, and APOE ε4 carrier status [58]. These findings indicate that brain clocks intended for disease research should not be evaluated solely on the basis of age-prediction accuracy. The robustness of the correspondence between their outputs and the target pathology or functional changes must also be established.

Region-specific modeling improves local age estimation but complicates comparisons across brain regions. Several existing clocks substantially underestimated cerebellar age, with greater bias among models trained without brain-related tissues [59]. Even when modeling was restricted to age-associated CpGs shared by the cerebellum and middle temporal gyrus, clocks trained separately on cerebellar and cerebral cortical samples showed systematic biases in opposite directions when applied across regions. The study further developed BrainCortexClock using both cerebellar and cortical samples and observed no consistent overestimation or underestimation of either region in an independent dataset [59]. These findings suggest that including different brain regions during model training and using their shared age-related signals can place regional age estimates on a more comparable scale. However, model output remains jointly shaped by local methylation trajectories and the tissue composition of the training data. Predicted ages generated by different models and regional differences in DNA methylation therefore cannot be directly interpreted as differences in the overall pace of biological aging across brain regions.

Cellular and spatial studies have shifted the question from whether brain tissue exhibits age acceleration to which cell populations and local environments contribute to the observed signals. Cell type–resolved methylation studies have detected AD-associated age acceleration in both neurons and glial cells, with more pronounced effects in temporal-lobe glia [60]. In progressive multiple sclerosis (MS), glia-enriched nuclear fractions have also shown age acceleration that was not detected in bulk brain tissue [61]. Single-nucleus transcriptomic clocks further identified different disease-associated patterns in independent postmortem datasets. In samples with high AD pathology, significant age acceleration was consistently detected in oligodendrocytes and microglia. In schizophrenia, acceleration was more widespread across major cell types, although microglial estimates showed relative age deceleration [62]. In preclinical studies of the mouse brain, spatial transcriptomic clocks have shown that cells located near T cells tend to have higher predicted ages, whereas those near neural stem cells tend to have lower predicted ages [38]. Taken together, human cell-type-resolved findings and preclinical spatial evidence suggest that clocks with cellular and spatial resolution may be useful for identifying patterns of vulnerability that are obscured in bulk tissue. The glial acceleration reported in AD and progressive MS, together with the relative microglial deceleration observed in schizophrenia, raises the possibility that glial aging patterns differ across neurological disorders. Comparative studies using consistent definitions of cell states and standardized neuropathological measures are needed to determine which patterns are shared and which are specific to individual diseases.

Brain-clock studies highlight the need to evaluate predictive calibration within a tissue, transportability across brain regions, and biological anchoring to disease-related processes as distinct forms of validity. Evidence for one form cannot substitute for evidence for the others.

3.2 Tissue-Adapted Clocks in Peripheral Organs

Evidence from the liver, kidney, cardiovascular system, and skeletal muscle shows that tissue-adapted age measures do not capture a single, uniform biological construct. Their interpretation depends on the biological level and molecular process represented, as well as the anatomical scope of the training data. The following subsections examine how these differences shape organ attribution and the validation claims supported by each model.

3.2.1 Divergent Hepatocyte-Related and Whole-Tissue Age Signals in the Liver

Liver aging involves both molecular changes within hepatocytes and remodeling of cellular composition and tissue architecture. Hepatocyte-related clocks and bulk-tissue clocks may therefore capture age-related changes at different biological levels. HepClock, which was developed using cell-type deconvolution, improved age estimation in primary hepatocytes and detected hepatocyte-related age acceleration more consistently than pan-tissue clocks across pathological contexts including nonalcoholic fatty liver disease, severe obesity, and α1-antitrypsin deficiency [60]. However, in a small study of liver biopsies from individuals with metabolic dysfunction–associated steatotic liver disease (MASLD), age acceleration estimated by the Horvath pan-tissue clock was associated with overall disease stage, steatosis, hepatocyte ballooning, and fibrosis. LiverClock was associated only with overall MASLD stage, whereas HepClock and the Horvath measure adjusted for cell composition showed no significant associations [63]. The differing results indicate that cell composition is part of the signal captured by bulk liver clocks. In MASLD, hepatocyte and cholangiocyte fractions decrease while endothelial cells, Kupffer cells, and lymphocytes increase, and these shifts track histological severity [63]. Adjustment for cell composition may therefore remove information that is relevant to tissue remodeling, even as it isolates variation that is less dependent on estimated cell proportions. Bulk tissue clocks and HepClock should consequently be interpreted as complementary measures. Reporting these estimates alongside quantitative histology and cell composition would help determine whether an observed age deviation primarily reflects aging within hepatocytes or remodeling of the tissue environment.

3.2.2 Complementary Kidney Aging Signals from DNA Methylation and Telomere Length

The central question in kidney aging-clock research is not which measure represents a complete "kidney age," but which age-related tissue changes are captured by each measure. Paired comparisons within the same donors showed that kidney tissue had higher DNA methylation age and age acceleration than peripheral blood, despite having longer telomeres [64]. This divergence indicates that DNA methylation age and telomere length are not redundant measures of the same dimension of aging. The former reflects epigenetic changes that accumulate with age, whereas the latter is influenced more strongly by cellular replicative history and telomere-maintenance processes.

EpiAge is a DNA methylation model developed to estimate chronological age in kidney tissue, whereas EpiKTL estimates kidney telomere length from kidney DNA methylation. In an additional set of 71 kidney tissue samples with matching histology, lower values of both measures were associated with greater nephrosclerosis, and each association persisted in models that included the other measure [65]. The inverse EpiAge association may reflect selective representation of residual tissue. Nephrosclerosis involves glomerular sclerosis, tubular atrophy, interstitial fibrosis, and arterial narrowing. EpiAge is calculated from DNA in cells that remain in the specimen, whereas cells lost during parenchymal atrophy and deposited extracellular matrix do not contribute to its signal. Injured human kidneys also contain reparative epithelial, stromal, and immune states around atrophic tubules and fibrotic regions [66]. As these populations become relatively more represented, their methylation profiles may shift the bulk EpiAge estimate downward even as structural damage accumulates. Adjustment for broad renal cell proportions cannot fully account for absent tissue or disease-specific cell states. The lower EpiAge estimate may therefore reflect which cells remain available for measurement rather than a biologically younger kidney. This explanation is provisional and could be tested by relating EpiAge to individual histological lesions and resolved injury states. EpiKTL is less ambiguous in direction because lower estimates correspond to shorter telomeres, which were directly associated with greater renal structural damage.

3.2.3 Disease Context and Phenotype Dependence of Cardiovascular Clock Associations

A cardiac methylation clock developed from right atrial

appendage tissue obtained from patients undergoing aortic valve replacement or coronary artery bypass grafting showed a lower mean cardiac age gap in the valve replacement group. Yet within this group, participants in the accelerated age gap category had larger left ventricular end-diastolic and end-systolic volumes, greater stroke volume, and a larger left ventricular internal diameter in diastole, while ejection fraction did not differ [67]. These findings are not directly contradictory because they refer to different comparisons. The group mean contrasts the valve replacement and bypass groups, whereas the echocardiographic analysis identifies ventricular differences associated with the accelerated age gap category within the valve replacement group. A lower average age gap at the group level therefore does not exclude an association between a higher age gap and altered ventricular measures within that group. At the same time, this association cannot be used to rank the overall severity of valvular and ischemic disease on a common scale. Differences in mechanical conditions between the two clinical settings were proposed as a possible explanation for this context dependence, but they were not directly tested. The absence of age-matched healthy cardiac tissue limits interpretation beyond these surgical cohorts.

Vascular findings show that the relationship between an age gap and vascular function depends on both the selected endpoint and the vascular region. In mice, the aortic age gap was associated with endothelial dysfunction in the abdominal aorta and femoral artery after adjustment for chronological age, but not in the thoracic aorta. No consistent association was found with pulse wave velocity [68]. The different associations with endothelial function and pulse wave velocity may reflect the age-related timing of these phenotypes. Endothelial dysfunction was evident from 36 weeks, whereas pulse wave velocity increased significantly only at 48 and 96 weeks. The aortic age gap may therefore be more closely aligned with the earlier appearing endothelial phenotype than with arterial stiffness. Because the study compared different age groups rather than repeated measurements from the same animals, this temporal sequence remains inferred rather than directly observed. Phenotype timing cannot, however, explain the absence of an association in the thoracic aorta, where endothelial dysfunction was also evident from 36 weeks. This finding suggests that regional factors also modify the relationship between the aortic age gap and vascular function.

3.2.4 Predictive Stability and Phenotype Sensitivity in Muscle Aging Models

The Muscle Epigenetic Age Test (MEAT) was developed from multiple skeletal muscle datasets and substantially improved chronological age prediction relative to the Horvath pan-tissue clock [69]. MEAT2.0 subsequently expanded the training sample and dataset coverage but achieved only a modest reduction in prediction error [70]. Although the two versions showed similar overall prediction accuracy, their selected CpGs overlapped only partially. The authors attributed this limited overlap to the large pool of age-associated CpGs from which elastic net models can select alternative combinations with comparable predictive performance. The comparison therefore separates predictive stability from feature stability because similar performance did not depend on retention of the same CpG set. More recent models based on next-generation sequencing and single base extension data from postmortem pectoralis major samples in a South Korean cohort also achieved good chronological age prediction [71]. These targeted CpG models were developed and tested within the same assembled cohort, providing additional evidence for skeletal-muscle model development but not independent external validation.

Age gaps derived from MEAT and other clocks were subsequently examined in relation to physical activity, physical function, and body composition in two independent Finnish cohorts [72]. Most associations were weak or absent after adjustment for sex and smoking. Higher physical activity was associated with larger Horvath or GrimAge age gaps for some activity measures, whereas the MEAT age gap was not associated with physical activity. Measures of physical function were also not consistently associated with muscle age gaps. These results complicate a uniformly adverse interpretation of the muscle age gap. If a larger muscle age gap is interpreted as poorer physiological status, it should generally accompany lower activity or worse function. Instead, the observed associations were predominantly null and occasionally pointed in the opposite direction. One plausible explanation is that physical activity modifies muscle methylation through remodeling and adaptation, which are not equivalent to the structural and functional deterioration associated with aging. A larger muscle age gap cannot currently be assigned a uniformly adverse physiological meaning.

MskAge used a broader modeling strategy that combined blood with multiple musculoskeletal tissues and cell types, including bone, cartilage, skeletal muscle, tendon, and mesenchymal stromal cells. In cell culture datasets, predicted age decreased during cellular reprogramming and increased during serial passage [73]. MskAge also yielded higher predicted age in lesioned osteoarthritic cartilage in selected comparisons, whereas no significant response was observed in the skeletal muscle exercise data examined. This contrast suggests that the observable response of MskAge may depend on both tissue context and the magnitude of the biological

perturbation. Reprogramming, serial passage, osteoarthritic lesions, and exercise differ substantially in experimental design and biological scale, so these findings do not establish that MskAge is inherently more sensitive to pathological than physiological change. Current evidence supports its responsiveness to pronounced cell state transitions and selected local cartilage differences, while its ability to track physiological adaptation in intact human skeletal muscle remains unresolved.

3.3 Clocks in Environmentally Exposed Organs: Lung, Gut, and Skin

3.3.1 Lung Aging Clocks

Current lung studies span bulk-tissue, cell type–resolved, and compartment-specific approaches. In idiopathic pulmonary fibrosis, several DNA methylation clocks indicated age acceleration, while DunedinPACE showed a faster pace of aging in regions with more severe pathological involvement [74], relating methylation measures to the regional burden of established fibrosis. ORANGE modeled chronological age from bulk GTEx lung transcriptomes and evaluated the model in independent samples annotated as normal lung tissue [75], addressing age prediction at the whole-tissue level without locating predictive information in particular cell populations or pathological regions.

Single-cell studies have begun to resolve which cellular compartments carry lung age signals. An earlier scRNA-seq study found that the cell types providing the strongest donor age prediction differed by smoking status, with epithelial populations most informative in nonsmokers and smooth muscle and endothelial populations in smokers [76]. Xu et al. subsequently integrated large-scale single-cell and spatial transcriptomic data from human lung parenchyma and trained an age-prediction model on cell type–resolved gene expression modules [77]. This model outperformed a comparably trained bulk-tissue model and retained its predictive accuracy in two independent single-cell datasets, and its most informative features corresponded to age-associated inflammatory and mitochondrial modules identified in the same study. The same analysis also documented substantial age-related shifts in lung cell composition, including declining alveolar epithelial and macrophage populations and expanding T cell and stromal populations.

A complementary methylation-based approach constructed separate clocks for airway epithelium and pulmonary parenchyma by projecting methylation profiles onto biological pathways [78]. Both clocks reproduced age prediction across independent cohorts, and age acceleration was associated with smoking burden, inhaled corticosteroid exposure, serum IgE levels, and disease severity across chronic obstructive pulmonary disease, idiopathic pulmonary fibrosis, and asthma datasets. These associations are cross-sectional, and pathway-level attribution remains a model-based decomposition rather than direct measurement of pathway activity. Current lung evidence spans bulk-tissue, cell type–resolved, and compartment-specific models whose reported features and associations are consistent with declining epithelial regenerative capacity and chronic immune activation; whether their age gaps track longitudinal change in lung pathology or function remains to be established.

3.3.2 Gut Aging Clocks

Early molecular approaches to gut aging often relied on microbial and experimental epithelial models rather than direct measurements from human intestinal tissue. Microbiome-based models predicted host chronological age from stool metatranscriptomic or metagenomic features [79, 80]. These approaches therefore characterize age-related variation in the gut microbial ecosystem rather than direct molecular aging of intestinal epithelial tissue. Human intestinal organoids retained donor-associated DNA methylation age in vitro, with small-intestinal organoids showing lower epigenetic age estimates than colonic organoids [81], suggesting segment-specific epithelial age-associated signals along the gut.

Two recent studies have developed DNA methylation clocks directly from human colon tissue. Sagy et al. constructed a colon-specific clock from CpG sites with colon-unique methylation patterns and achieved accurate chronological age prediction in healthy colon tissue. The age-related signal showed proximal–distal anatomical organization, consistent with segmental differences observed in intestinal organoids [81, 82]. Applied to disease datasets, the model estimated higher colonic age in HIV infection and in adult but not pediatric ulcerative colitis, suggesting context-dependent alterations in colonic molecular aging. Colonic polyps showed the largest estimated deviation, although these estimates extended beyond the training age range and should therefore be interpreted cautiously.

Schultz et al. developed a colon mucosa clock from healthy controls with equal representation of Black and White participants (termed EpiAge by its developers and distinct from the kidney EpiAge model discussed in Section 3.2.2) [83]. Histologically normal tissue adjacent to colorectal tumors showed significantly lower predicted age than control mucosa, and mitotic-clock measures indicated fewer stem-cell divisions in adjacent tissue. The authors interpreted these lower estimates as reflecting

altered stem-cell representation and a shift toward tumor-like molecular identity rather than a biologically younger mucosa. The direction of disease association differs between the two colon studies. Premalignant polyps appeared epigenetically older, whereas tumor-adjacent normal mucosa appeared younger. These comparisons involve different tissue contexts and are not directly contradictory, but they indicate that a colon age gap does not yet have a uniform direction or biological meaning across pathological settings. Current gut evidence includes microbial and organoid models as well as more recent human tissue-derived clocks with cross-sectional disease associations.

3.3.3 Skin Aging Clocks

Current skin-aging studies span bulk-skin and epidermal models; more recent work has used non-invasive tape stripping for epidermal sampling, while one model has targeted visual age rather than chronological age. Jiang et al. developed the skin-specific PathwayAge framework from bulk-skin DNA methylation profiles and evaluated age prediction across independent skin cohorts [84]. The model was subsequently applied to sun-exposed skin and several pathological states, with higher age acceleration observed in sun-exposed skin, actinic keratosis (AK), cutaneous squamous cell carcinoma (cSCC), and lesional psoriasis. In melanoma, overall age acceleration did not distinguish primary from metastatic tumors, although pathway-level analyses identified substantial remodeling of stress, immune, structural, and metabolic programs. These analyses extend skin age prediction toward pathway-level interpretation, although the female-only development cohort and predominance of bulk-tissue datasets limit resolution of layer- and cell-specific effects.

An earlier skin-specific DNA methylation (DNAm) predictor developed by Boroni et al. combined dermal, epidermal, and whole-skin methylation profiles and reproduced chronological age prediction in an independent whole-skin cohort [85]. Disease-associated age deviations, however, differed from those later observed with PathwayAge: lesional psoriatic skin appeared epigenetically younger than paired uninvolved skin, and AK also showed lower age estimates than healthy epidermis. These results are not directly contradictory because the models differ in training data, feature construction, and reference populations, but they indicate that skin age gaps do not yet have a uniform biological interpretation across pathological settings. Boroni et al. also applied the model to in vitro reprogramming experiments in cultured human fibroblasts and to senotherapeutic experiments in cultured fibroblasts and ex vivo human skin biopsies, although several treatment-associated changes in DNAm age were modest or nonsignificant.

Other approaches have focused more specifically on epidermal or visible aging phenotypes. Bienkowska et al. developed VisAgeX from epidermal methylation data to predict the difference between expert-rated visual facial age and chronological age and evaluated it in independent datasets [86]. This makes VisAgeX better interpreted as a phenotype-focused skin-aging measure than as a general tissue-age estimator. Menendez Vazquez et al. subsequently developed MitraSolo and MitraCluster from non-invasively tape-stripped epidermis [87]. These models showed reproducible age prediction across repeated sampling and independent datasets and also responded to cellular reprogramming, although this experimental setting does not establish that epidermal age gaps track longitudinal changes in intact human skin.

More recent work has examined cross-population generalizability and intervention response. Qi et al. developed an epidermis-specific DNA methylation clock that retained age-prediction performance in a multi-ethnic dataset [88]. In the same study, epidermal DNAm age decreased during an eight-week topical product-use study and was accompanied by improvements in visible and structural skin measures. However, the study used a prospective single-cohort design without a vehicle-control arm, limiting causal attribution of the methylation-age change to the tested formulation.

Skin-aging models have progressed from biopsy-derived chronological-age predictors toward pathway-based bulk-skin models, phenotype-anchored measures, and non-invasively sampled epidermal clocks. These models capture partly different constructs, and even skin-specific clocks can yield different age-gap directions in similar pathological settings. Whether these measures consistently track longitudinal deterioration or recovery of skin function therefore remains to be established.

3.4 Summary of Findings Across Organs

Across the organs reviewed, molecular aging clocks capture different biological levels and should not be interpreted as interchangeable measures of a single organ aging process. Central nervous system studies show that age estimates vary with brain region, cell population, and spatial context, emphasizing the need to distinguish predictive calibration from localization of age-related signals. In peripheral organs, comparisons among bulk-tissue, cell-focused, and alternative molecular measures similarly indicate that model output depends on the biological compartment and process represented. In the lung, gut, and skin, environmental exposure, tissue compartment, and sampling strategy further shape the signals captured by aging models.

Across these settings, chronological-age prediction is generally better established than the biological interpretation of the resulting age gaps. Differences in signal localization, model construction, and validation evidence need to be considered before organ age estimates are compared or translated across settings.

4. From Organ Age Gaps to Cross-Organ Networks and Translational Validation

Organ age gaps are used to compare aging patterns across organs, construct cross-organ networks, and evaluate associations with disease and clinical outcomes. These applications require separate consideration of how the age gap is defined, what generates dependence among organ estimates, and what level of validation supports the resulting biological or clinical claims.

4.1 Statistical Definitions of Age Gap and Their Implications for Cross-Organ Interpretation

Age gap generally denotes the deviation of model-predicted age from chronological age, but its statistical definition is not uniform. The direct difference between predicted and chronological age may be termed the raw age gap; the residual obtained by regressing predicted age on chronological age is commonly referred to as residual age acceleration; and the difference obtained after correcting for age-related bias or recalibrating the model may be termed the bias-corrected or calibrated age gap [10, 89]. These measures are not equivalent in statistical scale, dependence on chronological age, or comparability across cohorts and should not be treated as interchangeable. Their statistical definitions, interpretive implications, and considerations for cross-cohort, longitudinal, and cross-organ comparisons are summarized in Supplementary Table S3, together with the specific age-gap and related biological-age deviation measures identified in the reviewed evidence. For concision, we use age gap as an umbrella term for these measures, while results from individual studies should still be interpreted according to their original statistical definitions. Age-prediction models frequently exhibit regression toward the mean, whereby predicted age tends to be overestimated in younger individuals and underestimated in older individuals [89]. Without appropriate correction for age-related bias, the age gap may retain a systematic dependence on chronological age, thereby affecting its biological interpretation and cross-study comparison. Even when the same statistical definition is used, direct numerical comparison of age gaps across studies is generally not justified without broadly consistent model construction, preprocessing, training age ranges, and calibration procedures. Beyond these statistical considerations, an age gap does not represent a single biological component; it may reflect organ-intrinsic aging signals, shifts in cellular composition, shared systemic signals, disease-related remodeling, and technical or model-related variation (Fig. 2). These components may overlap or interact and generally cannot be fully disentangled using currently available data. This decomposition is therefore intended to define the interpretive boundaries of the age gap rather than to provide a directly estimable additive formula. Its interpretation must still be informed by the signal source and the available validation evidence.

These limitations in age-gap comparability and biological interpretation become particularly important when age gaps are compared across organs. Multi-organ proteomic studies have identified correlations among organ-associated age gaps, and elevated age gaps across multiple models have been associated with greater disease burden and mortality risk [48]. Such correlations may reflect biological coupling or shared systemic influences. They may also be shaped by shared elements of model construction. Organ models trained against the same chronological-age target may draw on overlapping molecular features, while common preprocessing, batch effects, and calibration procedures can contribute to correlated model outputs. Cross-organ networks derived from these measures should be interpreted as patterns of statistical dependence rather than direct evidence of communication between organs. A separate limitation concerns directionality. Because most organ age estimates have been obtained at the same visit, these associations do not establish temporal ordering or identify an upstream organ. Even when temporal precedence is demonstrated longitudinally, additional evidence would still be required to support causality because unmeasured common causes and time-varying confounding can generate similar patterns.

4.2 From Disease Association to Clinical Validation

If clinical translation is the intended goal, validation should be aligned with the intended use and should draw on multiple complementary domains of evidence [19–21]. These domains include reproducibility in independent cohorts and across platforms, direct anchoring to the pathology or function of the target organ, prospective prediction of disease onset or functional decline, longitudinal responsiveness to intervention, and evidence that use of the measure improves clinical decision-making. External validation should distinguish numerical transportability from the transportability of biological interpretation. A fixed model may preserve calibration and chronological-age prediction across cohorts while the

direction or magnitude of its age-gap association with target organ pathology or function changes. Both forms of transportability should be evaluated separately. At the disease-association stage, differences in age gap between patients and healthy individuals may represent a risk signal preceding disease onset, but they may also result from the pathological process, treatment exposure, or changes in tissue composition. Because most clocks were developed to predict chronological age rather than to measure treatment response, their suitability for intervention studies cannot be inferred from age prediction accuracy or cross-sectional associations with disease. These domains inform validation maturity within the S–R–V framework, whereas analytical validity of the measurement process remains a separate prerequisite.

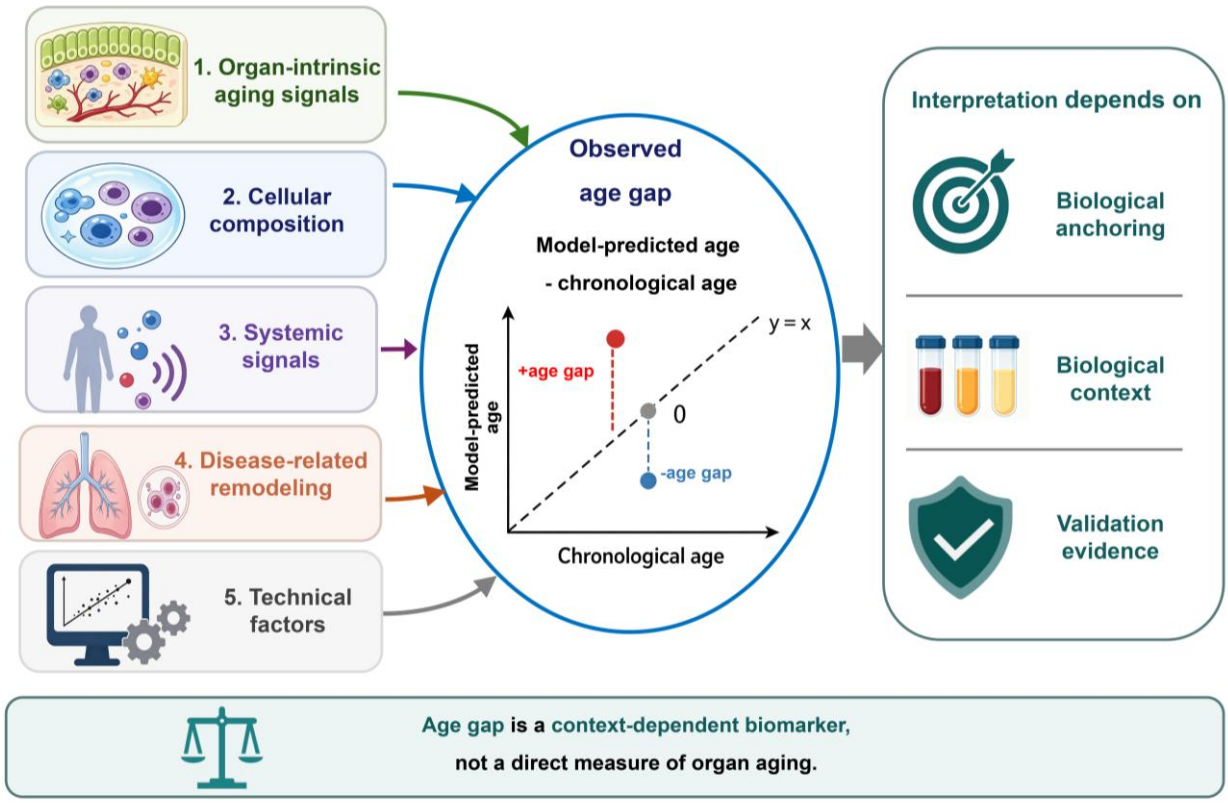


Figure 2. Biological and technical determinants of observed age gap estimates. The central plot illustrates the raw age gap, defined as model-predicted age minus chronological age. Positive and negative values indicate that predicted age is higher or lower than chronological age, respectively. Residual age acceleration is typically defined as the residual from regressing predicted age on chronological age, whereas calibrated or bias-corrected measures adjust systematic age-related prediction error using study-specific procedures. Throughout this review, the term age gap is used broadly as an umbrella term encompassing raw, residual, calibrated, and bias-corrected age gap measures. Supplementary Table S3 summarizes their definitions and the specific age-gap measures identified in the reviewed evidence. An observed age gap may reflect organ-intrinsic aging signals, cellular composition, systemic signals, disease-related remodeling, and technical or model-related variation. Its interpretation therefore depends on biological anchoring, biological context, and validation evidence rather than representing a direct measure of organ aging.

Analytical validity concerns the end-to-end measurement process, including preanalytical sample handling, assay measurement, and computational processing [19]. Sources of variation should be distinguished because preanalytical and assay effects, batch or platform effects, computational-pipeline choices, and recalibration can alter model output without representing biological change. These technical sources should in turn be distinguished from within-person biological variation, which reflects genuine temporal variation in the measured biological state but does not necessarily indicate a sustained change in organ aging. Before an organ age measure is used for longitudinal monitoring, intervention evaluation, or clinical practice, its output should therefore be characterized under both repeatability and reproducibility conditions, with

attention to stability across relevant batches, platforms, and computational implementations. A low mean absolute error or successful replication of an age association does not establish that a small within-person change in model output reflects a true change in biological aging rather than technical variation or short-term biological variability. Across the representative models reviewed here, direct estimates of final-output repeatability or technical variance were uncommon, within-person variability was rarely assessed, and no formal minimum detectable change threshold was identified (Supplementary Table S4). For applications in which change over time is interpreted, the minimum detectable change should be established and related to corresponding biological, functional, or clinical change.

Proximal fluids and peripheral circulating proxies show why predictive replication must be distinguished from biological validation. A cerebrospinal fluid proteomic clock captured age-related patterns involving synaptic processes, inflammation, and injury repair and retained its age-prediction performance in an independent Alzheimer's Disease Neuroimaging Initiative (ADNI) cohort [44]. However, its signals integrate contributions from multiple central nervous system compartments, and its age gap did not differ between matched cognitively normal amyloid-β–positive and amyloid-β–negative individuals. Thus, transportability of age prediction does not necessarily imply sensitivity to preclinical amyloid status [44]. Multi-organ plasma proteomic models have been replicated across populations and platforms [48, 90–92], and their organ age gaps have been examined in relation to age-related diseases, multimorbidity, cognitive changes, and mortality [93–96]. Together, these studies support the reproducibility of circulating proxy models and their associations with health outcomes, but do not establish that within-person changes in these proxies consistently track molecular aging, pathological progression, or functional decline in the corresponding solid tissues.

Prospective validation should determine whether an organ age gap predicts disease onset, pathological progression, or functional decline related to the target organ and whether its predictive effect is independent of chronological age and major confounders. When multiple clocks or organ age gaps are evaluated against numerous outcomes, analyses should prespecify the relevant family of tests and apply a multiplicity strategy appropriate to the study objective [97]. Effect estimates and confidence intervals should be reported for both null and statistically significant findings. If risk stratification is the intended use, studies should assess whether the age gap improves calibration, discrimination, or clinical net benefit beyond lifestyle factors, routine laboratory measures, and conventional assessments of organ function [98].

For longitudinal or intervention use, changes in an age gap should be shown to correspond to changes in target organ function or relevant clinical outcomes. Clinical utility can be considered only when use of the measure improves a predefined clinical or trial decision. The relevance of individual validation domains depends on the intended use of the measure. A model that supports risk stratification may not be suitable for longitudinal monitoring or intervention evaluation, because these uses place different demands on calibration, analytical stability, within-person responsiveness, and biological or clinical anchoring. S–R–V profiles should be interpreted together with a specified context of use rather than reduced to a single hierarchy of validation maturity. Evidence established for one intended use should not be assumed to support another.

4.3 Roadmap for Future Research

Future studies should prioritize paired datasets that link, within the same individuals, molecular measures from the target tissue, proximal fluids, and peripheral circulation with organ-specific pathological or functional endpoints. Such datasets would allow investigators to determine whether different measurement pathways reflect corresponding biological changes. For solid tissues that cannot be sampled repeatedly, clinical biopsies or surgical specimens may provide a tissue anchor. Autopsy studies should, where possible, link postmortem tissue findings to premortem fluid biomarkers and organ function data. On this basis, repeatedly accessible fluid measures could be used for follow-up at multiple time points to examine within-person changes in age gap and their temporal relationships with functional decline, pathological progression, and disease onset.

To assess directionality, integrated multi-organ studies should collect repeated measurements at intervals matched to the expected dynamics of each organ. Analyses should test whether the baseline age gap or interval change in one organ predicts subsequent change in another after accounting for prior values in both organs and measured shared systemic factors. Candidate temporal relationships should be replicated in independent populations and, where feasible, examined during interventions with a well-characterized primary target. These designs could help distinguish temporal coupling between organs from correlations generated by common systemic change. Figure 3 summarizes the proposed paired longitudinal validation design.

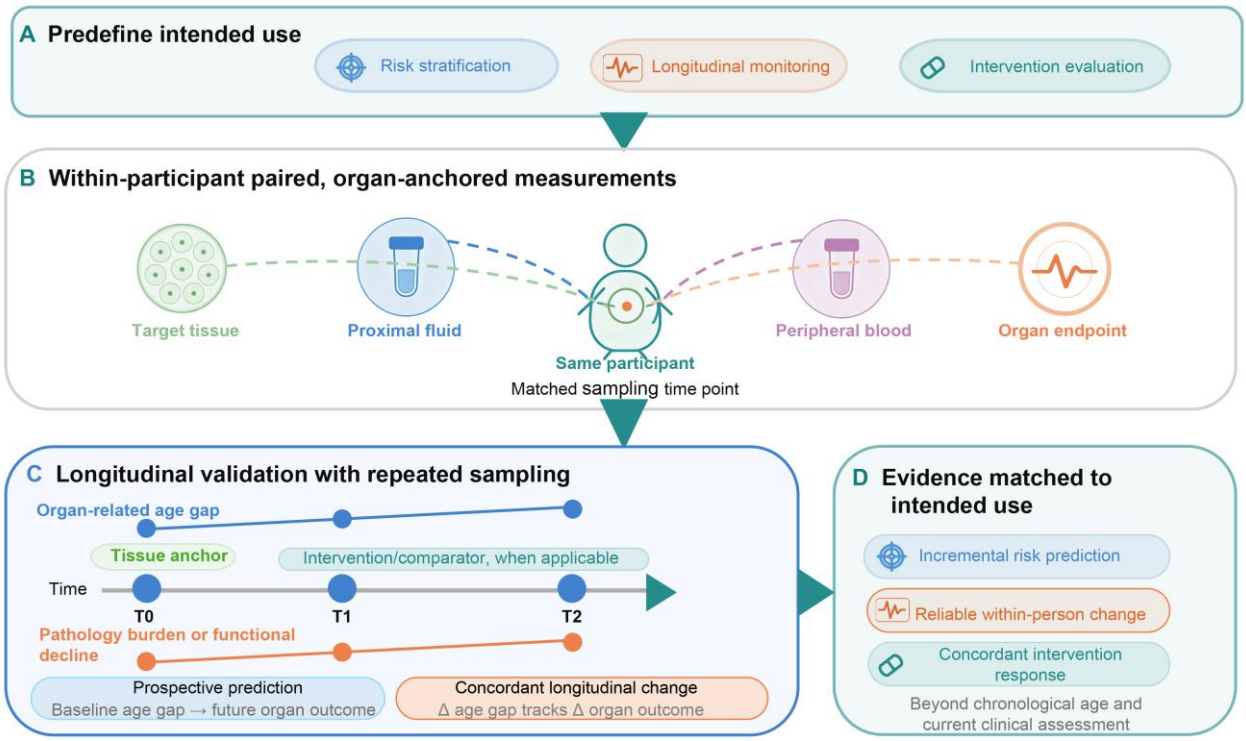


Figure 3. A paired longitudinal validation design for organ-related molecular aging clocks. A predefined intended use is specified first **(A)**, including risk stratification, longitudinal monitoring, or intervention evaluation. Within the same participant, target tissue, proximal fluid, peripheral blood, and a corresponding organ endpoint are measured in a paired, organ-anchored manner, ideally at the same sampling time point **(B)**. Longitudinal validation uses repeated sampling from baseline (T0) through follow-up time points (e.g., T1 and T2), with tissue anchoring at baseline and intervention or comparator conditions when applicable, to evaluate prospective prediction and concordant longitudinal change between the organ-related age gap and the organ endpoint **(C)**. Evidence is interpreted according to the intended use **(D)**: risk stratification requires evidence of incremental risk prediction, longitudinal monitoring requires reliable within-person change, and intervention evaluation requires concordant intervention response. These validation outcomes aim to determine whether the age gap provides information beyond chronological age and current clinical assessment. In panel C, the blue trajectory represents the organ-related age gap and the orange trajectory represents the corresponding organ endpoint; the trajectories are illustrative and do not indicate improvement or deterioration. Δ denotes within-participant change.

Beyond these design priorities, artificial intelligence (AI), particularly deep-learning approaches, may extend molecular aging models by capturing nonlinear relationships, learning from high-dimensional data, and integrating multiple data types [99–101]. However, complex models may remain difficult to interpret, may inherit biases and technical variation from their training data, and still require external and biological validation before their outputs are generalized or used clinically [100, 102]. AI-derived aging measures should therefore be independently replicated, transparently reported, and rigorously audited, with clinical use guided by expected benefit, patient safety, and legal and ethical responsibilities [99, 102, 103].

4.4 Review Limitations and Scope of the Framework

As a critical narrative review, this article may be affected by publication bias and literature-selection bias. The organs and molecular modalities covered are representative rather than exhaustive and include both organs for which tissue-adapted models have been developed and organs with a substantially more limited evidence base. Organ age measures based on imaging, physiological measurements, or clinical scores were not emphasized because they fall outside the scope of molecular aging clocks defined in this review. Organs differ substantially in sample source, molecular modality, study size, and validation endpoint; the available evidence therefore does not support a simple cross-organ ranking of model performance.

Population generalizability remains uneven across tissue- and organ-related molecular aging models. Ancestral and geographic coverage has historically been asymmetric, with much of the earlier evidence derived from Western populations and more limited evaluation in non-European populations [48, 104]. This gap is narrowing. Organ-attributed proteomic clocks developed in the UK Biobank have now been externally evaluated in Chinese and U.S. cohorts, and related models have been

developed directly in a large East Asian cohort [90, 104]. Age representation is similarly heterogeneous. Several large cohort-based and clinically sampled studies are concentrated in middle-to-late adulthood, whereas other tissue-specific models span much broader age ranges. A broad age range does not necessarily ensure adequate representation across the life course, and models may still be less reliable in sparsely sampled age groups [48, 57]. Sampling frame adds another layer of heterogeneity. Access to less-accessible internal tissues often depends on autopsy, clinically indicated surgery, or disease-related biopsy [67], which can enrich study populations for particular ages and clinical conditions. Newer studies using healthy-donor tissue and minimally or non-invasively sampled tissues are beginning to broaden direct-tissue evidence [83, 87]. Together, these patterns indicate that generalizability should be evaluated rather than assumed. Future studies should report demographic and age distributions clearly, examine prediction error and calibration across relevant population strata when adequately powered, and test fixed models in geographically and ancestrally diverse independent cohorts.

The S–R–V framework structures model comparison without generating a composite score. For organs with currently limited evidence, our assessments indicate that sufficient support has not yet been established; they do not demonstrate the absence of a measurable organ-related aging signal.

5. Conclusions

Across the studies reviewed, molecular age measures were associated with different aspects of organ state and did not support a single biological interpretation across organs. The S–R–V framework distinguishes the anatomical source and biological resolution of an aging estimate from the validation domains that have been evaluated, without treating these dimensions as evidence of organ specificity or clinical utility by themselves. Current evidence is concentrated in age prediction, independent evaluation, and cross-sectional associations with established tissue states, whereas prospective, longitudinal, intervention, and decision-impact evidence remains less developed. Stronger organ-specific or translational claims require analytically reproducible measurement, independent evaluation of the fixed model, and biological anchoring to the target organ, together with evidence appropriate to the intended use. Organ-specific attribution additionally requires evidence distinguishing the target organ signal from shared systemic or other organ sources. Translational claims also require evidence of added value beyond chronological age and established clinical measures. No single S–R–V category is sufficient for these claims; the required evidence should instead be interpreted in relation to the model and its specified context of use.

Funding

This work was supported by the Medical Research Project of Chongqing Municipal Science and Technology Commission and Health Commission (grant number: 2026MSXM004), the Scientific Research Project of Yongchuan Hospital Affiliated to Chongqing Medical University (grant number: YJJL2024070), the Scientific Research Project of Yongchuan Hospital Affiliated to Chongqing Medical University (grant number: YJJL201705), and the Chongqing Public Health Key Specialty (Discipline) Project.

Conflict of Interest

The authors declare no conflicts of interest.

Acknowledgments

The authors used ChatGPT to translate an author-written Chinese draft into English and to assist with English language editing. The authors reviewed and revised the resulting text and take full responsibility for the manuscript's content, accuracy, and references.

Supplementary Materials

The Supplementary data can be found online at: www.aginganddisease.org/EN/10.14336/AD.2026.1010.

References

[1] Beard JR, Officer A, De Carvalho IA, Sadana R, Pot AM, Michel J-P, et al. (2016). The world report on ageing and health: A policy framework for healthy ageing. The Lancet, 387:2145–2154.

[2] López-Otín C, Blasco MA, Partridge L, Serrano M, Kroemer G (2023). Hallmarks of aging: An expanding universe. Cell, 186:243–278.

[3] Hannum G, Guinney J, Zhao L, Zhang L, Hughes G, Sadda S, et al. (2013). Genome-wide methylation profiles reveal quantitative views of human aging rates. Mol Cell, 49:359–367.

[4] Horvath S (2013). DNA methylation age of human tissues and cell types. Genome Biol, 14:R115.

[5] Chen BH, Marioni RE, Colicino E, Peters MJ, Ward-Caviness CK, Tsai P-C, et al. (2016). DNA methylation-based measures of biological age: Meta-analysis predicting time to death. Aging, 8:1844–1865.

[6] Fransquet PD, Wrigglesworth J, Woods RL, Ernst ME, Ryan J (2019). The epigenetic clock as a predictor of disease and mortality risk: A systematic review and meta-analysis. Clin Epigenetics, 11:62.

[7] Levine ME, Lu AT, Quach A, Chen BH, Assimes TL, Bandinelli S, et al. (2018). An epigenetic biomarker of aging for lifespan and healthspan. Aging, 10:573–591.

[8] Lu AT, Quach A, Wilson JG, Reiner AP, Aviv A, Raj K, et al. (2019). DNA methylation GrimAge strongly predicts lifespan and healthspan. Aging, 11:303–327.

[9] Belsky DW, Caspi A, Corcoran DL, Sugden K, Poulton R, Arseneault L, et al. (2022). DunedinPACE, a DNA methylation biomarker of the pace of aging. Elife, 11:e73420.

[10] Higgins-Chen AT, Thrush KL, Wang Y, Minteer CJ, Kuo P-L, Wang M, et al. (2022). A computational solution for bolstering reliability of epigenetic clocks: Implications for clinical trials and longitudinal tracking. Nat Aging, 2:644–661.

[11] Li J, Jiang B, Zhang W, Hao J, Liu Z, Ji Q, et al. (2026). Multimodal clocks of human aging. Cell, 189:4489-4511.e31.

[12] The GTEx Consortium, Aguet F, Anand S, Ardlie KG, Gabriel S, Getz GA, et al. (2020). The GTEx consortium atlas of genetic regulatory effects across human tissues. Science, 369:1318–1330.

[13] Bennett DA, Buchman AS, Boyle PA, Barnes LL, Wilson RS, Schneider JA (2018). Religious orders study and rush memory and aging project. J Alzheimers Dis, 64:S161–S189.

[14] Zhang K, Hocker JD, Miller M, Hou X, Chiou J, Poirion OB, et al. (2021). A single-cell atlas of chromatin accessibility in the human genome. Cell, 184:5985-6001.e19.

[15] Loyfer N, Magenheim J, Peretz A, Cann G, Bredno J, Klochendler A, et al. (2023). A DNA methylation atlas of normal human cell types. Nature, 613:355–364.

[16] Wyss-Coray T, Topol EJ (2026). Biological aging clocks in health and disease. Nat Med, 32:2383–2394.

[17] Zalesky A, Wen J, Tian YE (2026). From whole-body to organ-specific biological age clocks. Nat Aging, 6:961–969.

[18] Niu J, Peng Y, Yin L, Wu M (2026). Quantum sensing for precision organ aging assessment. Aging Dis. doi: 10.14336/AD.2025.1500.

[19] FDA-NIH Biomarker Working Group BEST (biomarkers, EndpointS, and other tools) resource. Food and Drug Administration (US): Silver Spring (MD); 2016.

[20] Moqri M, Herzog C, Poganik JR, Justice J, Belsky DW, Higgins-Chen A, et al. (2023). Biomarkers of aging for the identification and evaluation of longevity interventions. Cell, 186:3758–3775.

[21] Moqri M, Herzog C, Poganik JR, Ying K, Justice JN, Belsky DW, et al. (2024). Validation of biomarkers of aging. Nat Med, 30:360–372.

[22] Field AE, Robertson NA, Wang T, Havas A, Ideker T, Adams PD (2018). DNA methylation clocks in aging: Categories, causes, and consequences. Mol Cell, 71:882–895.

[23] Jaffe AE, Irizarry RA (2014). Accounting for cellular heterogeneity is critical in epigenome-wide association studies. Genome Biol, 15:R31.

[24] Houseman EA, Accomando WP, Koestler DC, Christensen BC, Marsit CJ, Nelson HH, et al. (2012). DNA methylation arrays as surrogate measures of cell mixture distribution. BMC Bioinformatics, 13:86.

[25] Vellame DS, Shireby G, MacCalman A, Dempster EL, Burrage J, Gorrie-Stone T, et al. (2023). Uncertainty quantification of reference-based cellular deconvolution algorithms. Epigenetics, 18:2137659.

[26] Teschendorff AE, Zheng SC (2017). Cell-type deconvolution in epigenome-wide association studies: A review and recommendations. Epigenomics, 9:757–768.

[27] Zheng SC, Breeze CE, Beck S, Teschendorff AE (2018). Identification of differentially methylated cell types in epigenome-wide association studies. Nat Methods, 15:1059–1066.

[28] Yang X, Zhao F, Ren T, Chen C, Byrne KT, Danilov AV, et al. (2025). OmicsTweezer: A distribution-independent cell deconvolution model for multi-omics data. Cell Genomics, 5:100950.

[29] Li W, Zhang Z, Kumar S, Botey-Bataller J, Zoodsma M, Ehsani A, et al. (2025). Single-cell immune aging clocks reveal inter-individual heterogeneity during infection and vaccination. Nat Aging, 5:607–621.

[30] Mao S, Su J, Wang L, Bo X, Li C, Chen H (2023). A transcriptome-based single-cell biological age model and resource for tissue-specific aging measures. Genome Res, 33:1381–1394.

[31] Xie G (2026). scAgeClock: A single-cell transcriptome-based human aging clock model using gated multi-head attention neural networks. Npj Aging, 12:75.

[32] Zhu X, Lin Y, Li J, Wang J, Peng X (2021). ScDA: A denoising AutoEncoder based dimensionality reduction for single-cell RNA-seq data. In: Wei Y, Li M, Skums P, Cai Z, editors Bioinforma. Res. Appl. Cham: Springer International Publishing, 534–545.

[33] Tran HTN, Ang KS, Chevrier M, Zhang X, Lee NYS, Goh M, et al. (2020). A benchmark of batch-effect correction methods for single-cell RNA sequencing data. Genome Biol, 21:12.

[34] Abdelaal T, Michielsen L, Cats D, Hoogduin D, Mei H, Reinders MJT, et al. (2019). A comparison of automatic cell identification methods for single-cell RNA sequencing data. Genome Biol, 20:194.

[35] Zimmerman KD, Espeland MA, Langefeld CD (2021). A practical solution to pseudoreplication bias in single-cell studies. Nat Commun, 12:738.

[36] Liu D-D, Hu H-Y, Li F-F, Hu Q-Y, Liu M-W, Hao Y-J, et al. (2025). Spatial transcriptomics meets diabetic kidney disease: Illuminating the path to precision medicine. World J Diabetes, 16:107663.

[37] Allen WE, Blosser TR, Sullivan ZA, Dulac C, Zhuang X (2023). Molecular and spatial signatures of mouse brain aging at single-cell resolution. Cell, 186:194-208.e18.

[38] Sun ED, Zhou OY, Hauptschein M, Rappoport N, Xu L, Navarro Negredo P, et al. (2025). Spatial transcriptomic clocks reveal cell proximity effects in brain ageing. Nature, 638:160–171.

[39] Chen KH, Boettiger AN, Moffitt JR, Wang S, Zhuang X (2015). Spatially resolved, highly multiplexed RNA profiling in single cells. Science, 348:aaa6090.

[40] Hu J, Li X, Coleman K, Schroeder A, Ma N, Irwin DJ, et al. (2021). SpaGCN: Integrating gene expression, spatial location and histology to identify spatial domains and spatially variable genes by graph convolutional network. Nat Methods, 18:1342–1351.

[41] Palla G, Spitzer H, Klein M, Fischer D, Schaar AC, Kuemmerle LB, et al. (2022). Squidpy: A scalable framework for spatial omics analysis. Nat Methods, 19:171–178.

[42] Denisenko E, Guo BB, Jones M, Hou R, De Kock L, Lassmann T, et al. (2020). Systematic assessment of tissue dissociation and storage biases in single-cell and single-nucleus RNA-seq workflows. Genome Biol, 21:130.

[43] Ferreira PG, Muñoz-Aguirre M, Reverter F, Sá Godinho CP, Sousa A, Amadoz A, et al. (2018). The effects of death and post-mortem cold ischemia on human tissue transcriptomes. Nat Commun, 9:490.

[44] Melendez J, Sung YJ, Orr M, Yoo A, Schindler S, Cruchaga C, et al. (2024). An interpretable machine learning-based cerebrospinal fluid proteomics clock for predicting age reveals novel insights into brain aging. Aging Cell, 23:e14230.

[45] Farinas A, Rutledge J, Bot VA, Western D, Ying K, Lawrence KA, et al. (2025). Disruption of the cerebrospinal fluid–plasma protein balance in cognitive impairment and aging. Nat Med, 31:2578–2589.

[46] Rooney MR, Chen J, Ballantyne CM, Hoogeveen RC, Boerwinkle E, Yu B, et al. (2025). Correlations within and between highly multiplexed proteomic assays of human plasma. Clin Chem, 71:677–687.

[47] Lehallier B, Gate D, Schaum N, Nanasi T, Lee SE, Yousef H, et al. (2019). Undulating changes in human plasma proteome profiles across the lifespan. Nat Med, 25:1843–1850.

[48] Oh HS-H, Rutledge J, Nachun D, Pálovics R, Abiose O, Moran-Losada P, et al. (2023). Organ aging signatures in the plasma proteome track health and disease. Nature, 624:164–172.

[49] Basisty N, Kale A, Jeon OH, Kuehnemann C, Payne T, Rao C, et al. (2020). A proteomic atlas of senescence-associated secretomes for aging biomarker development. PLOS Biol, 18:e3000599.

[50] Sun BB, Maranville JC, Peters JE, Stacey D, Staley JR, Blackshaw J, et al. (2018). Genomic atlas of the human plasma proteome. Nature, 558:73–79.

[51] Tarkhov AE, Lindstrom-Vautrin T, Zhang S, Ying K, Moqri M, Zhang B, et al. (2024). Nature of epigenetic aging from a single-cell perspective. Nat Aging, 4:854–870.

[52] Meyer DH, Schumacher B (2024). Aging clocks based on accumulating stochastic variation. Nat Aging, 4:871–885.

[53] Tong H, Dwaraka VB, Chen Q, Luo Q, Lasky-Su JA, Smith R, et al. (2024). Quantifying the stochastic component of epigenetic aging. Nat Aging, 4:886–901.

[54] Schaum N, Lehallier B, Hahn O, Pálovics R, Hosseinzadeh S, Lee SE, et al. (2020). Ageing hallmarks exhibit organ-specific temporal signatures. Nature, 583:596–602.

[55] Takasugi M, Nonaka Y, Takemura K, Yoshida Y, Stein F, Schwarz JJ, et al. (2024). An atlas of the aging mouse proteome reveals the features of age-related post-transcriptional dysregulation. Nat Commun, 15:8520.

[56] Grodstein F, Lemos B, Yu L, Klein H-U, Iatrou A, Buchman AS, et al. (2021). The association of epigenetic clocks in brain tissue with brain pathologies and common aging phenotypes. Neurobiol Dis, 157:105428.

[57] Shireby GL, Davies JP, Francis PT, Burrage J, Walker EM, Neilson GWA, et al. (2020). Recalibrating the epigenetic clock: Implications for assessing biological age in the human cortex. Brain, 143:3763–3775.

[58] Thrush KL, Bennett DA, Gaiteri C, Horvath S, Dyck CHV, Higgins-Chen AT, et al. (2022). Aging the brain: Multi-region methylation principal component based clock in the context of alzheimer's disease. Aging, 14:5641–5668.

[59] Wang Y, Grant OA, Zhai X, Mcdonald-Maier KD, Schalkwyk LC (2024). Insights into ageing rates comparison across tissues from recalibrating cerebellum DNA methylation clock. Geroscience, 46:39–56.

[60] Tong H, Guo X, Jacques M, Luo Q, Eynon N, Teschendorff AE (2024). Cell-type specific epigenetic clocks to quantify biological age at cell-type resolution. Aging, 16:13452–13504.

[61] Kular L, Klose D, Urdánoz-Casado A, Ewing E, Planell N, Gomez-Cabrero D, et al. (2022). Epigenetic clock indicates accelerated aging in glial cells of progressive multiple sclerosis patients. Front Aging Neurosci, 14:926468.

[62] Muralidharan C, Zakar-Polyák E, Adami A, Abbas AA, Sharma Y, Garza R, et al. (2025). Human brain cell-type-specific aging clocks based on single-nuclei transcriptomics. Adv Sci, 12:e06109.

[63] Van Dijck E, Van Laere S, Logie E, Timmermans S, Fransen E, Ibrahim J, et al. (2025). Gradual DNA methylation changes reveal transcription factors implicated in metabolic dysfunction-associated steatotic liver disease progression and epigenetic age acceleration. Clin Epigenetics, 17:138.

[64] Pavanello S, Campisi M, Rigotti P, Bello MD, Nuzzolese E, Neri F, et al. (2022). DNA methylation - and telomere - based biological age estimation as markers of biological aging in donors kidneys. Front Med, 9:832411.

[65] Akinnibosun OA, Xu XG, Emmett A, Nguyen H, Hames-Fathi S, Drzal M, et al. (2026). Shorter kidney telomeres are associated with nephrosclerosis by an epigenetic signature. Cardiovasc Res, 122:607–620.

[66] Lake BB, Menon R, Winfree S, Hu Q, Melo Ferreira R, Kalhor K, et al. (2023). An atlas of healthy and injured cell states and niches in the human kidney. Nature, 619:585–594.

[67] Mongelli A, Panunzi S, Nesta M, Gottardi Zamperla M, Atlante S, Barbi V, et al. (2023). Distinguishable DNA

methylation defines a cardiac-specific epigenetic clock. Clin Epigenetics, 15:53.

[68] Pośpiech E, Bar A, Pisarek-Pacek A, Karaś A, Branicki W, Chlopicki S (2024). Epigenetic clock in the aorta and age-related endothelial dysfunction in mice. Geroscience, 46:3993–4002.

[69] Voisin S, Harvey NR, Haupt LM, Griffiths LR, Ashton KJ, Coffey VG, et al. (2020). An epigenetic clock for human skeletal muscle. J Cachexia Sarcopenia Muscle, 11:887–898.

[70] Voisin S, Jacques M, Landen S, Harvey NR, Haupt LM, Griffiths LR, et al. (2021). Meta-analysis of genome-wide DNA methylation and integrative omics of age in human skeletal muscle. J Cachexia Sarcopenia Muscle, 12:1064–1078.

[71] Yang S-B, Lee JM, Kim M-Y, Lee SD, Lee HY (2025). Epigenetic aging signatures and age prediction in human skeletal muscle. Aging, 17:2809–2843.

[72] Sillanpää E, Heikkinen A, Kankaanpää A, Paavilainen A, Kujala UM, Tammelin TH, et al. (2021). Blood and skeletal muscle ageing determined by epigenetic clocks and their associations with physical activity and functioning. Clin Epigenetics, 13:110.

[73] Green DC, Reynard LN, Henstock JR, Reppe S, Gautvik K, Peffers MJ, et al. (2025). MskAge —an epigenetic biomarker of musculoskeletal age derived from a genetic algorithm islands model. Aging Cell, 24:e70149.

[74] Kurbanov DB, Ahangari F, Adams T, De Man R, Tang J, Carlon M, et al. (2025). Epigenetic age acceleration in idiopathic pulmonary fibrosis revealed by DNA methylation clocks. Am J Physiol-Lung Cell Mol Physiol, 328:L456–L462.

[75] Jalal W, Musarrat M, Samee MAH, Rahman MS (2026). ORANGE: A machine learning approach for modeling tissue-specific aging from transcriptomic data. Brief Bioinform, 27:bbag093.

[76] Song Q, Singh A, McDonough JE, Adams TS, Vos R, De Man R, et al. (2024). Predicting lung aging using scRNA-seq data. PLOS Comput Biol, 20:e1012632.

[77] Xu K, Kim GS, Bhagwat A, Meimand SE, Venkat VV, Pham G, et al. (2026). Cellular hallmarks and aging clock of the human lung parenchyma. Nat Commun, 17:8680.

[78] Liao J, Huang Z, Liu Y, Cai F, Zhu J, Wang S, et al. (2026). An epithelial-derived epigenetic clock reveals pathway-level aging mechanisms in chronic lung disease. Npj Aging. doi: 10.1038/s41514-026-00487-2.

[79] Gopu V, Camacho FR, Toma R, Torres PJ, Cai Y, Krishnan S, et al. (2024). An accurate aging clock developed from large-scale gut microbiome and human gene expression data. iScience, 27:108538.

[80] Fu J, Zhang J, He R, Dong Q, Mao H, Shen W, et al. (2026). A global metagenomic atlas of aging identifies a microbiota phase transition associated with disease risk. Npj Biofilms Microbiomes, 12:97.

[81] Lewis SK, Nachun D, Martin MG, Horvath S, Coppola G, Jones DL (2020). DNA methylation analysis validates organoids as a viable model for studying human intestinal aging. Cell Mol Gastroenterol Hepatol, 9:527–541.

[82] Sagy N, Bender O, Bar DZ (2026). Colon-specific epigenetic clocks from minimal features reveal disease-driven aging. Sci Rep. doi: 10.1038/s41598-026-64349-3.

[83] Schultz BM, Ayeotan O, Rana JN, Litwin S, Basickes S, Sapienza C, et al. (2026). Abnormal epigenetic aging of epigenetic outliers in normal colon mucosa from colorectal cancer patients. Sci Rep, 16:4022.

[84] Jiang J, Li P, Zhu J, Cai F, Wang S, Huang Z, et al. (2026). Pathway-level insights into the epigenetic ageing of human skin. Age Ageing, 55:afag118.

[85] Boroni M, Zonari A, Reis de Oliveira C, Alkatib K, Ochoa Cruz EA, Brace LE, et al. (2020). Highly accurate skin-specific methylome analysis algorithm as a platform to screen and validate therapeutics for healthy aging. Clin Epigenetics, 12:105.

[86] Bienkowska A, Raddatz G, Söhle J, Kristof B, Völzke H, Gallinat S, et al. (2024). Development of an epigenetic clock to predict visual age progression of human skin. Front Aging, 4:1258183.

[87] Menendez Vazquez A, Katsanos D, Vasile M, Graham A, Dyster V, Kaveh S, et al. (2025). Epigenetic age predictors for non-invasive assessment of human skin. Npj Aging, 12:11.

[88] Qi M, Pitta P, Wegner K, Kristof B, Feng Y, Raddatz G, et al. (2026). Epigenetic skin aging and its reversal to improve skin longevity across ethnicities and phototypes using a dihydromyricetin-containing serum: Results from a prospective, single-cohort study. Dermatol Ther, 16:3049–3064.

[89] Salih A, Nichols T, Szabo L, Petersen SE, Raisi-Estabragh Z (2023). Conceptual overview of biological age estimation. Aging Dis, 14:583–588.

[90] Wang Y, Xiao S, Liu B, Jiang R, Liu Y, Hang Y, et al. (2026). Organ-specific proteomic aging clocks predict disease and longevity across diverse populations. Nat Aging, 6:162–180.

[91] Oh HS-H, Le Guen Y, Rappoport N, Urey DY, Farinas A, Rutledge J, et al. (2025). Plasma proteomics links brain and immune system aging with healthspan and longevity. Nat Med, 31:2703–2711.

[92] Goeminne LJE, Vladimirova A, Eames A, Tyshkovskiy A, Argentieri MA, Ying K, et al. (2025). Plasma protein-based organ-specific aging and mortality models unveil diseases as accelerated aging of organismal systems. Cell Metab, 37:205-222.e6.

[93] Zhao R, Lu H, Yuan H, Chen S, Xu K, Zhang T, et al. (2025). Plasma proteomics-based organ-specific aging for all-cause mortality and cause-specific mortality: A prospective cohort study. Geroscience, 47:1411–1423.

[94] Kang S, Baker S, Hayhoe B, Price G, Novak G, Wong J, et al. (2025). Organ-specific proteomic aging and cognitive performance: Implications for risk prediction of alzheimer's disease and related dementias in older adults. J Prev Alzheimers Dis, 12:100274.

[95] Robinson O, Xiao H, Homann J, Viallon V, Ferrari P, Frank P, et al. (2026). Associations of proteomic age clocks with lifestyle risk factors, incident chronic diseases and mortality in two european cohorts. Nat Aging, 6:1437–1451.

[96] Kivimäki M, Frank P, Pentti J, Jokela M, Nyberg ST, Blake A, et al. (2025). Proteomic organ-specific ageing signatures and 20-year risk of age-related diseases: The whitehall II observational cohort study. Lancet Digit Health, 7:e195–e204.

[97] Bender R, Lange S (2001). Adjusting for multiple testing—when and how? J Clin Epidemiol, 54:343–349.

[98] Steyerberg EW, Vickers AJ, Cook NR, Gerds T, Gonen M, Obuchowski N, et al. (2010). Assessing the performance of prediction models: A framework for traditional and novel measures. Epidemiology, 21:128–138.

[99] Srour L, Bejaoui Y, She J, Alam T, El Hajj N (2025). Deep aging clocks: AI-powered strategies for biological age estimation. Ageing Res Rev, 112:102889.

[100] Wang G, Ding P, Li Z, Tang Q, Tu L, Jiang T, et al. (2026). Artificial intelligence approaches in biological age prediction: Current status and challenges. Br J Biomed Sci, 83:16141.

[101] Lin A, Giosan I, Aparicio A, Guo T, Melnikas M, Balagué-Dobón L, et al. (2026). DeepStrataAge: An interpretable deep-learning clock that reveals stage- and sex-divergent DNA methylation aging dynamics. Npj Aging, 12:62.

[102] Mahbub TB, Safaeian P, Sohrabi S (2026). A comprehensive review of artificial intelligence as a catalyst in aging research: Insights, gaps and future perspectives. Front Aging, 7:1644669.

[103] Babker AM (2026). Clinical safety and legal accountability of artificial intelligence in hematology diagnostic laboratories: Risks, failure modes, medicolegal challenges, and budgeting for implementation. J Appl Hematol, 17:85–92.

[104] Bennett DA, Wang B, Xiao S, Wright N, Edris A, Wang Y, et al. (2026). Proteomic organ-specific signatures, ageing traits, disease risks and genetic architecture in an east asian population. Ebiomedicine, 130:106401.

[105] McMurran CE, Karlsson IK, Mostafaei S, Wang Y, Gerritsen L, Pedersen NL, et al. (2025). Brain DNA Methylation Age, Lifestyle Factors and Dementia in the Swedish Twin Registry. Aging Cell, 24:e70117.

[106] Liu S, Huang Y, Park T, Lee EH, Chaudhuri S, Adzibolosu N, et al. (2025). Plasma proteomic alzheimer's risk score: Biological age clock and pseudotime trajectory. Alzheimers Dement, 21:e70851.

[107] Liu CS, Yeo W-J, Surapaneni A, Windham BG, Oh HS-H, Prizment A, et al. (2025). Biological organ ages associate with risk of chronic diseases in a community-based population. Jci Insight, 10:e197304.

[108] Mishra M, Kim H-H, Youm Y-H, Gonzalez-Hurtado E, Zaitsev K, Dlugos T, et al. (2026). Exoproteome of calorie-restricted humans identifies complement deactivation as an immunometabolic checkpoint reducing inflammaging. Nat Aging, 6:1064–1078.

[109] Heikkinen A, Uusitalo-Kylmälä L, Blom I, Helge JW, Gillberg L, Seaborne R, et al. (2026). The divergent effects of nicotinamide riboside and high-intensity exercise training on skeletal muscle epigenetic aging. Aging Cell, 25:e70638.

[110] Gorski PP, Raastad T, Ullrich M, Turner DC, Hallén J, Savari SI, et al. (2023). Aerobic exercise training resets the human skeletal muscle methylome 10 years after breast cancer treatment and survival. Faseb J, 37:e22720.

[111] Jankowski CM, Konigsberg IR, Wilson MP, Sun J, Brown TT, Julian CG, et al. (2024). Skeletal muscle DNA methylation: Effects of exercise and HIV. Aging Cell, 23:e14025.

[112] Nicholson T, Dhaliwal A, Quinlan JI, Allen SL, Williams FR, Hazeldine J, et al. (2024). Accelerated aging of skeletal muscle and the immune system in patients with chronic liver disease. Exp Mol Med, 56:1667–1681.

[113] Santamaria G, Iglesias C, Jung S, Arcos Hodar J, Nogueiras R, Del Sol A (2025). A machine-learning approach identifies rejuvenating interventions in the human brain. Adv Sci, 12:e03344.

[114] Seo D, Do AN, Heo G, Kwon J, Song S, Apio C, et al. (2025). Cerebrospinal fluid proteomic signatures in cognitively normal individuals identify distinct clusters linked to neurodegeneration. Nat Aging, 5:2125–2141.

[115] Hwangbo N, Zhang X, Raftery D, Gu H, Hu S-C, Montine TJ, et al. (2022). A metabolomic aging clock using human cerebrospinal fluid. J Gerontol A Biol Sci Med Sci, 77:744–754.

[116] Qu K, Dal Canto E, Van Ommen A-MLN, Kamar SA, Teske AJ, Cramer MJ, et al. (2025). Proteome organ aging and cardiometabolic risk in a population at risk for heart failure. Cardiovasc Diabetol, 24:430.

[117] Hong SB, Shin Y-W, Moon J, Park K-I, Jung K-Y, Cho K, et al. (2026). *In vivo* tau in epilepsy reflects clinical severity and immune- and ageing-related proteomic changes. Brain, awag145. doi: 10.1093/brain/awag145

[118] Nie C, Li Y, Li R, Yan Y, Zhang D, Li T, et al. (2022). Distinct biological ages of organs and systems identified from a multi-omics study. Cell Rep, 38:110459.

[119] Jia H, Chen X, Chang Y, Wang Y, Lindberg EL, Cui H, et al. (2026). Life-span–dependent transcriptional dynamics of the human heart. Sci Adv, 12:eaeg2614.

[120] Zhong Y, Xia M, Zhao X, Qu Y, Lei B, Zhen S, et al. (2026). Construction and validation of plasma protein-based musculoskeletal biological age and genetic and environmental risk profiles. Aging Cell, 25:e70636.

[121] Sarkar A, Liu NQ, Magallanes J, Tassey J, Lee S, Shkhyan R, et al. (2023). STAT3 promotes a youthful epigenetic state in articular chondrocytes. Aging Cell, 22:e13773.